Appl Phys B (2009) 96: 337–343
DOI 10.1007/s00340-009-3590-0

Applied Physics B
Lasers and Optics

Investigation on guided mode characteristics of hollow-core photonic band-gap fiber with interstitial holes from near-infrared to visible wavelengths

J.-H. Yuan · C.-X. Yu · X.-Z. Sang · G.-Y. Zhou · S.-G. Li · L.-T. Hou

Received: 16 January 2009 / Revised version: 7 April 2009 / Published online: 26 June 2009

Abstract Guided-mode characteristics of a hollow-core photonic band-gap fiber (HC-PBGF) fabricated by the improved twice stack-and-draw technique are investigated from near-infrared to visible wavelengths. The Full-Vector Plane-Wave Method (FVPWM) is employed to analyze the transverse field distributions in near-infrared wavelengths. The propagation mode fields in visible wavelengths are experimentally observed. The influences of glass interstitial apexes and interstitial holes on photonic band gaps and mode characteristics are analyzed. The possible degenerate state and loss mechanism of guided modes in photonic band gaps are elementarily discussed.

PACS 03.40.Kf · 42.81.Cn · 71.15.Ap

1 Introduction

Because of unique propagation characteristics [1, 2], the hollow-core photonic band-gap fiber (HC-PBGF), which confines light energy in air core by the Bragg scattering effect [3], has opened new strategies for high-field physics and nonlinear optics of ultrashort pulses [4–6]. During the past decade, the mode characteristics including the guided modes and cladding modes lying in or beyond the photonic band gaps (PBGs) have been theoretically and experimentally investigated. Cregan et al. first reported the hollow-core guidance in visible wavelengths corresponding to the higher-order band gaps [7]. Bouwmans et al. analyzed the properties of HC-PBGF at 850 nm, where the existing forms of different guided modes in the fundamental band gap were investigated [8]. Konorov et al. reported the dynamic propagation process of visible light in HC-PBGF and showed the transverse field distributions [9]. Couny et al. investigated the forming mechanism of band gaps and achieved the experimental visualization of the Bloch modes in HC-PBGF, where the relation between the guided modes and cladding modes was indicated [10]. In addition, they pointed out three kinds of resonators including the glass interstitial apexes, the silica structures between neighboring apexes and the air holes, and they showed the dominant contribution of the cladding modes to the upper-edge and lower-edge forming of band gaps through Bloch theory and two experimental procedures. As reported in [10], the glass interstitial apexes significantly influenced the positions of the band gaps and existing forms of guided modes.

Here, guided-mode characteristics of HC-PBGF with larger structure size fabricated in our lab are theoretically and experimentally investigated. Especially, the influence of the glass interstitial apexes on the forming of band gaps is analyzed, and the propagation possibility of such a HC-PBGF with interstitial holes is confirmed. Finally, the possible existing forms and loss mechanism of guided modes in band gaps are discussed.

J.-H. Yuan (✉) · C.-X. Yu · X.-Z. Sang
Key Laboratory of Information Photonics and Optical Communications, Ministry of Education, Beijing University of Posts and Telecommunications, 100876 Beijing, China
e-mail: yuanjinhui81@163.com
Fax: +86-106-2281162

G.-Y. Zhou · S.-G. Li · L.-T. Hou
Key Laboratory of Metastable Materials Science & Technology, Yanshan University, 066004 Qinghuangdao, China

2 Simulation and experiment

Figure 1 is the cross-section of HC-PBGF designed and fabricated by the improved twice stack-and-draw technique [11, 12]. This technique can keep the integrity of inner and outer cladding structures of HC-PBGF. As shown in Fig. 1(a), the whole cross section of HC-PBGF includes the outer cladding structure with diameter $D_1 = 320$ μm, which plays an important role in coupling the light energy into the inner cladding region and preventing it from leaking out, and the inner cladding structure with diameter $D_2 = 80$ μm, which can confine light energy in the air core to propagate along the longitudinal direction. In Fig. 1(b), the amplified inner cladding structure is shown, and the corresponding structure parameters are as follows: the average cladding air hole diameter $d = 3.9$ μm, hole to hole pitch $\Lambda = 4.16$ μm, and core diameter $D = 16.95$ μm. The irregular cladding and interstitial holes are formed due to fluctuations of temperature and surface tension in the process of fabrication.

In the simulation, all cladding and interstitial holes are considered to be of regular circularity with the same sizes. Because of the symmetrical structure, a quarter of the model cross section is shown as Fig. 2(a). The chosen structure parameters: the cladding air hole diameter $d = 3.9$ μm, interstitial holes diameter $d_{\text{int}} = 0.75$ μm, hole to hole pitch $\Lambda = 4.15$ μm, and core diameter $D = 17$ μm. The position and width of the band gaps as a function of air filling fraction is shown in Fig. 2(b), showing the influence of interstitial holes on the band-gap characteristics.

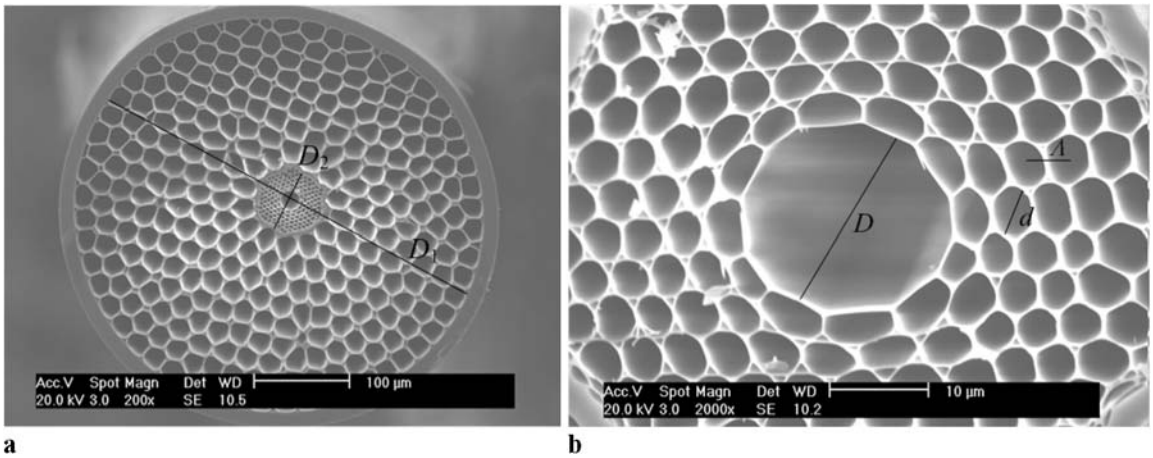

Fig. 1 (**a**) The whole cross section of HC-PBGF. (**b**) The amplified inner cladding structure

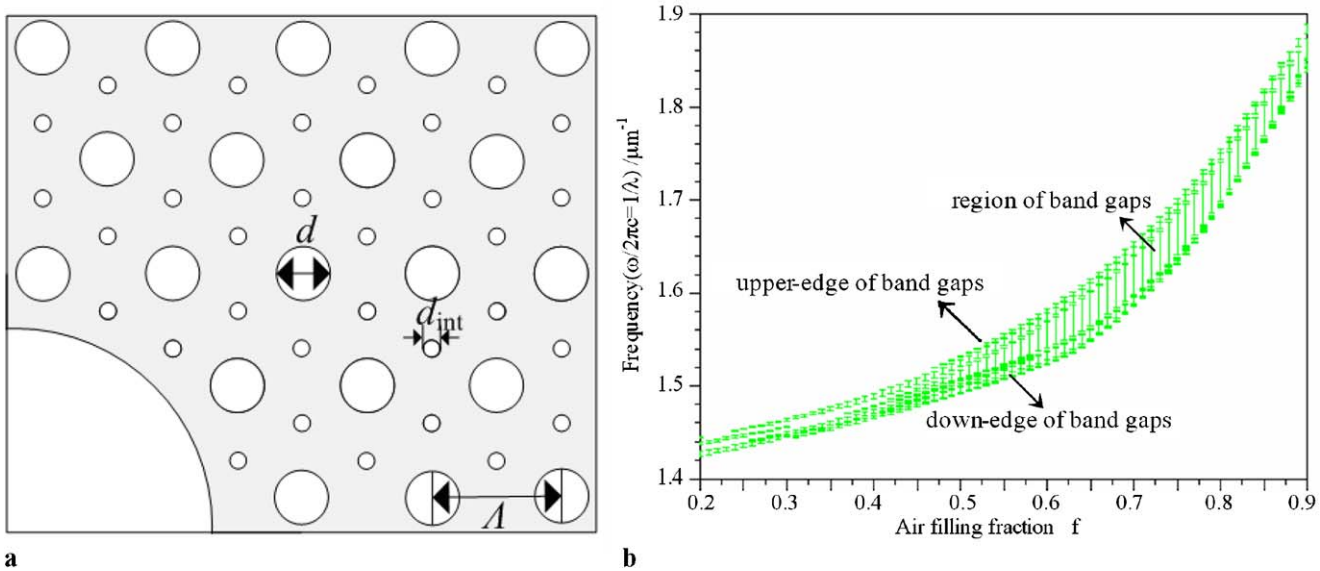

Fig. 2 (**a**) The model cross-section structure. (**b**) The positions of the band gaps as a function of air filling fraction, points and bars indicating the upper and down edges and the region of the band gaps, respectively

The upper edge of the band gaps depends on the resonance effect of the glass interstitial apexes, which play an important role in reflecting light energy with the same wavelength scale. When the air filling fraction achieves up to 95%, the interstitial apexes can be considered to be a series of isolated points, distributed symmetrically and periodically in air. The light energy whose wavelength satisfies the Bragg condition will be scattered back into the air core, and propagates along the longitudinal direction. Therefore, the characteristics of band gaps and mode field distributions are primarily dependent on the interstitial apex sizes, and the position of the band gaps will gradually shift to shorter wavelengths due to the existence of interstitial holes. As shown in Fig. 2(b), the position is more sensitive on air filling fraction from 0.5 to 0.9, and the slope can achieve up to 50% and 70% before and after 0.75. Based on the Full-Vector Plane-Wave Method (FVPWM) [13, 14], the normalized frequency $K\Lambda$ as a function of the normalized propagation constant $\beta\Lambda$ is shown in Fig. 3.

In Fig. 3, while $\beta\Lambda$ is varying from 24 to 52, $K\Lambda$ is an approximately linear function of $\beta\Lambda$ with the slope approaching 45°, and different order PBGs labeled as 1st, 2nd and 3rd are primarily considered. As illustrated in Fig. 3, the valid parts of three PBGs with $K\Lambda > \beta\Lambda$ (above air line) are existing in the $K\Lambda$ ranges from 26.5 to 30, 32.5 to 39.7 and 46.5 to 49.3, and the corresponding wavelength ranges are from 871 to 986 nm, 658 to 804 nm and 530 to 568 nm, respectively. There are true photonic states in these valid PBGs, and the photonic energy can be transmitted along the longitudinal direction in a defect core. Moreover, the guidance at a low attenuation in these valid PBGs arises from waveguide properties of identified structural cladding constituents and shows a similar mode spectrum as the fiber cladding. However, when $K\Lambda < \beta\Lambda$ is satisfied (below the air line), the photonic energy lying in PBGs leaks out into the cladding region, and it is distributed over the whole cross section including holes and glass structure, existing in the form of Bloch modes. In the insert, Γ-point, M-point, and J-point of the reciprocal lattice in the first Brillouin zone have different contributions to the upper- and down-edge forming of band gap (Γ-point for upper edge, M-point and J-point for down edge) [10]. Because of the two glass apexes existing within a primitive unit cell of the cladding crystal, the cladding modes at the Γ-point include symmetric or anti-symmetric modes. The symmetric modes, which are known as the modified fundamental space filling modes and form the upper edge of the in-of-plane band gaps (below the air line), are characterized by the fields in all the apexes being in-phase with one another. For anti-symmetric modes propagating in the air core, they form the upper edge of the out-of-plane band gaps (above the air line). However, it is impossible to sustain a single mode (the core diameter should be less than about 15 times the operational wavelength) due to a larger core diameter size, and the multiple mode characteristics are complicated. The propagation experiment is carried out, and the setup is shown in Fig. 4.

The lens system and coupling device are used to increase the coupling efficiency, and a linear CCD is responsible for monitoring the output state. The pinhole diaphragm

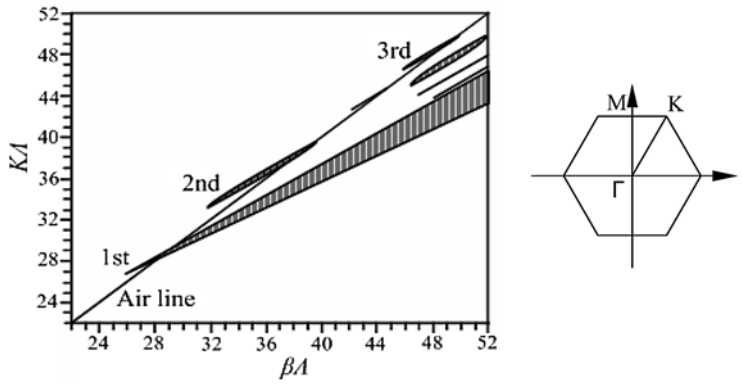

Fig. 3 The normalized frequency $K\Lambda$ as a function of the normalized propagation constant $\beta\Lambda$, 1st, 2nd and 3rd corresponding to the different order band gaps considered, and the *solid line* indicating the air line. The insert displays the first Brillouin zone symmetry point nomenclature

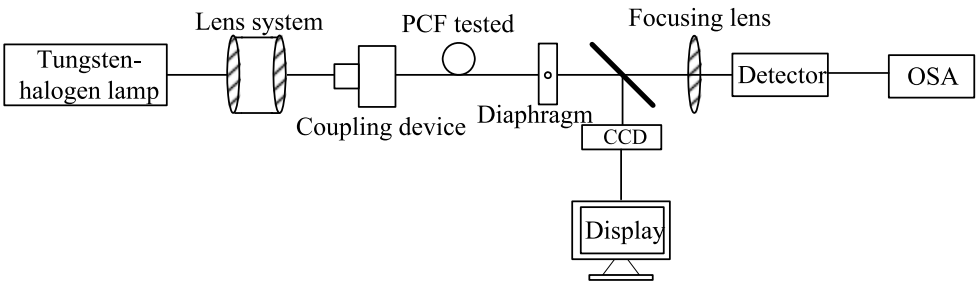

Fig. 4 The experiment setup

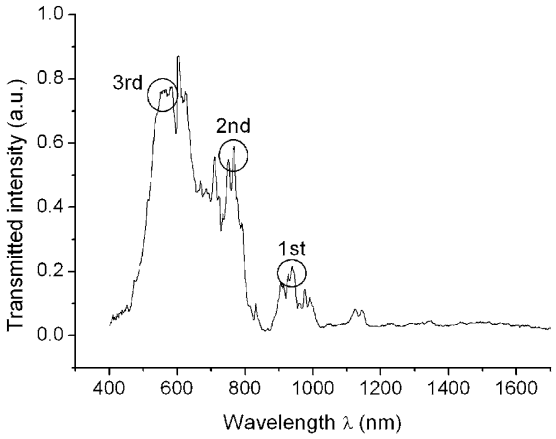

Fig. 5 The transmitted intensity in the air core as a function of wavelength, 1st, 2nd and 3rd associated with the *circles* corresponding to different order band gaps labeled in Fig. 3, respectively

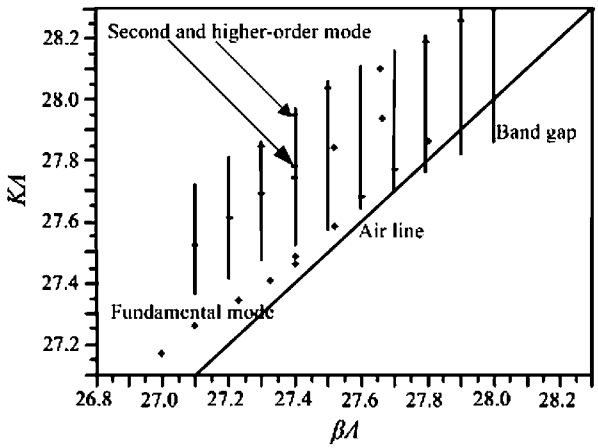

Fig. 6 The existing forms of the guided mode with $\beta\Lambda$ from 27 to 28, the *plus signs* standing for the fundamental, second-order (labeled by the *longer arrow*) and higher-order (labeled by the *shorter arrow*) guided modes, the *bars* and *solid line* indicating part of 1st band gap and the air line, respectively

only permits the energy in air core to enter into the optical spectrum analyzer (OSA). The length of HC-PBGF is about 0.65 m, and the propagation loss is measured to be less than 0.055 dB/m at 600 nm by the cut-back method. The transmission spectrum with wavelength range from 400 to 1700 nm measured by OSA is shown in Fig. 5.

As shown in Fig. 5, the 3 dB transmitted intensities of 1st, 2nd and 3rd PBGs correspond to the wavelength ranges from 895 to 980 nm, 705 to 795 nm and 525 to 580 nm. Comparing Fig. 5 with Fig. 3 (the corresponding wavelength ranges are from 871 to 986 nm, 658 to 804 nm and 530 to 568 nm, respectively), the upper and down edges of the band gaps occur to shift, and the primary reason is considered to be the approximation on shapes and sizes of cladding and interstitial holes in the simulation.

2.1 Simulation on guided mode characteristics in near-infrared wavelengths

The guided mode characteristics in near-infrared wavelengths from 895 to 980 nm, corresponding to the 1st PBG in Fig. 5, are theoretically investigated. The existing forms of different guided modes in part of the 1st PBG with $\beta\Lambda$ changing from 27 to 28 (corresponding to the wavelength range from 931 to 965 nm) are shown in Fig. 6.

The air guided modes can be classified into the fundamental, second-order and higher-order guided modes due to the discrepancy of the effective refractive index $n_{\text{eff}}(\beta/K)$. As illustrated in Fig. 6, the fundamental guided mode with n_{eff} above 0.99 within $\beta\Lambda$ changing from 27.5 to 27.8 may be well confined in the air core. The second-order guided mode with n_{eff} below 0.99 within $\beta\Lambda$ changing from 27.1 to 27.65 has a higher leakage loss as the propagation distance increases [15, 16]. Compared with the fundamental and second-order guided modes, the higher-order guided modes with n_{eff} below 0.98 within $\beta\Lambda$ changing from 27.3 to 27.9 may distribute all over the boundary between the air core and the cladding structure. The corresponding transverse field distributions are shown in Fig. 7.

In Fig. 7(a) and (b), the three and two dimension electric field intensity distributions of the fundamental guided mode with n_{eff} 0.99236 at $\beta\Lambda = 27.6$ reach a maximum at the center of the fiber core and monotonically decrease with the distance from the center. In Fig. 7(c), (d) and (e), compared to the fundamental guided mode, the electric field intensities of the second-order guided mode with n_{eff} 0.98335, the first higher-order guided mode with n_{eff} 0.97886, and second higher-order guided mode with n_{eff} 0.97125 at $\beta\Lambda = 27.6$ are becoming weaker and diffuse into the neighboring region, showing a higher propagation loss.

2.2 Experimental observation on guided modes in visible wavelengths

Four output near-fields in the wavelength ranges from 705 to 795 nm and 525 to 580 nm, corresponding to the 2nd and 3rd PBGs in Fig. 5, are observed using a line-array CCD through shielding the cladding region with a small hole diaphragm and adjusting the coupling efficiency from 45% to 55%, as shown in Fig. 8.

In Fig. 8, the red light ((a) and (b)) and green light ((c) and (d)) are propagating from the air core. Fig. 8(a) and (c) correspond to the observation without diaphragm, and the mode fields extend all over the whole cross section, the energy ratio between the air core and cladding region being about 0.5. Using a diaphragm to shield the energy from the cladding region, the output mode fields observed primarily come from the air core, as shown in Fig. 8(b) and (d). Although more details about the mode characteristics cannot

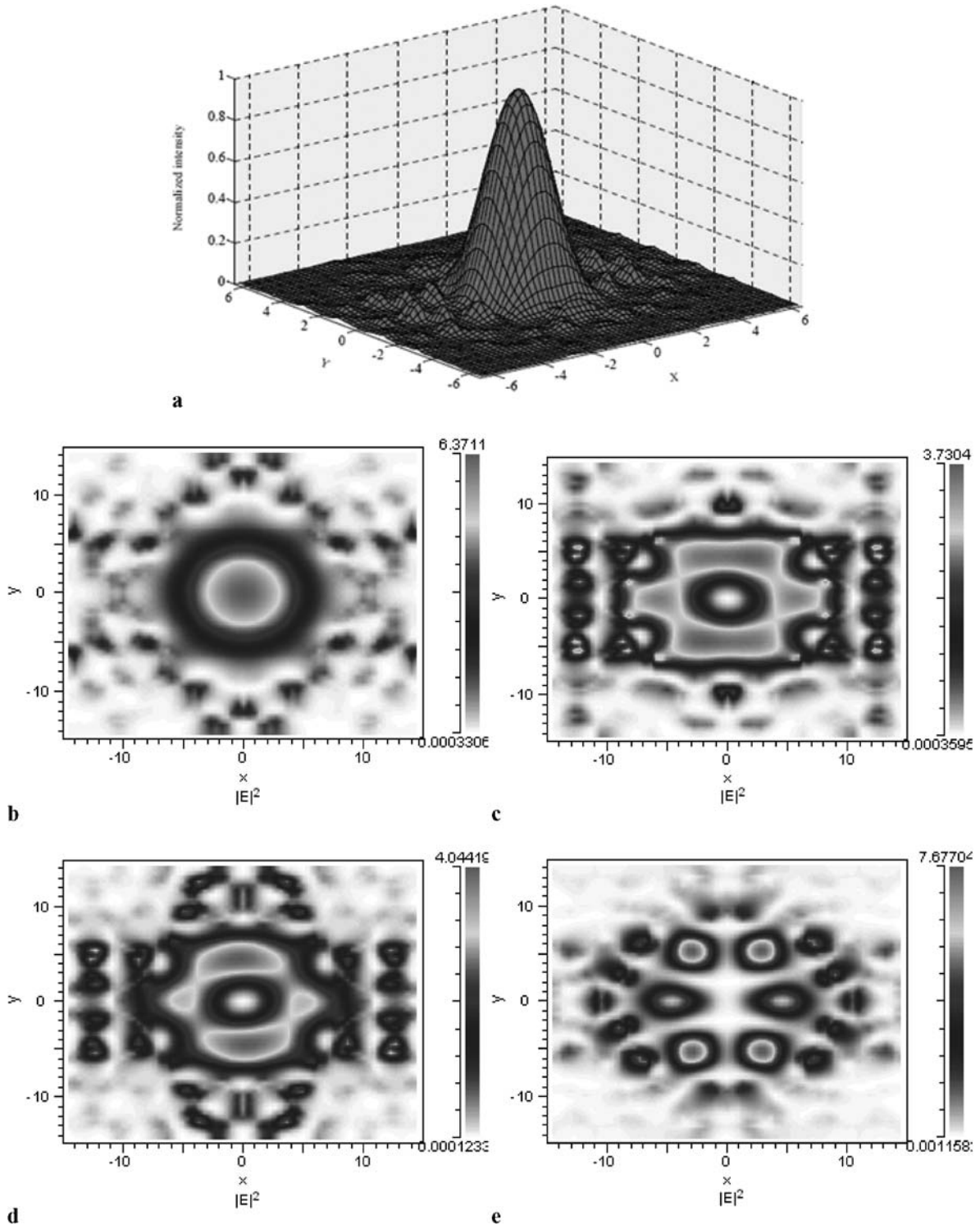

Fig. 7 The transverse field distributions of air guided modes, (**a**) and (**b**) displaying the two and three dimension distribution of the fundamental guided mode, (**c**), (**d**), and (**e**) displaying the distributions of second-order and higher-order guided modes, respectively

be distinguished due to the restriction of CCD resolution and a shorter HC-PBGF length, it is believed that the mixing modes including the fundamental and second-order guided modes at least are propagating in the air core.

3 Discussion of polarization states and loss

All kinds of guided modes caused by defect states of the transverse photonic lattice exist in different polarization and

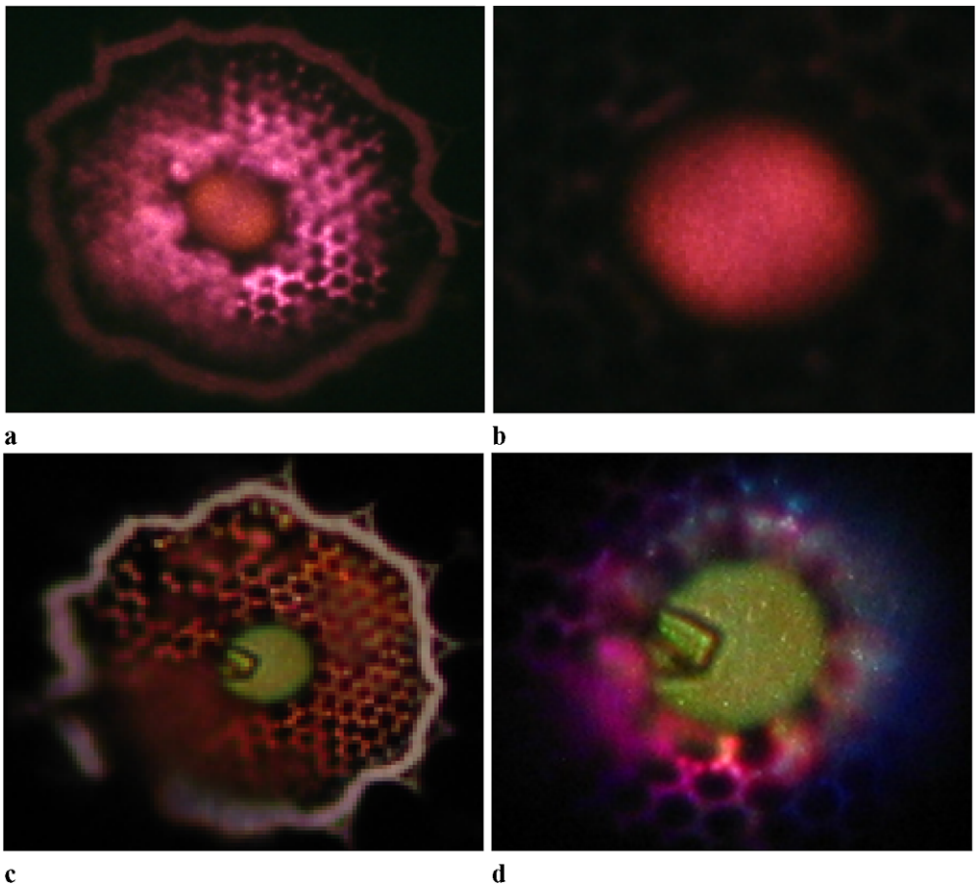

Fig. 8 The four output near-fields observed in experiment, (**a**) and (**b**) corresponding to the wavelength range from 705 to 795 nm, (**c**) and (**d**) corresponding to the wavelength range from 525 to 580 nm

degeneracy states. The fundamental guided mode consists of a degenerate pair of quasi-uniformly polarized states (the doublet of HE_{11} mode). As shown in Fig. 3, the fundamental guided mode with $\beta\Lambda$ changing from 27.0 to 27.4 is far outside the band gap and not especially well confined, and it tends to be noisier with more energy in the lattice part. At higher values of the propagation constant ($\beta\Lambda$ changes from 27.5 to 27.8), it falls into the band gap and can effectively propagate along the longitudinal direction. For any fiber with rotational symmetry of order greater than 2, every mode must either be one of a two-fold degenerate pair with hybrid quasi-uniform polarization, or else must be a single state (no degeneracy) of TE or TM polarization with a mode profile that supports all the symmetries of the fiber itself. The second-order guided mode is a four-fold degenerate state. In fact, the second mode consists of a degenerate pair of two-lobed modes (the doublet of HE_{21} mode), and two additional states are similar but they have different frequencies for TE and TM polarization (TE_0 and TM_0 mode). Moreover, these states combine to form the first and second LP mode (LP_{01} and LP_{11} mode), and it is similar to the Bloch-mode characteristics in the weak guidance theory of conventional step-index fibers, which is enhanced by the emergence of interstitial holes.

Compared with the losses of solid core photonic crystal fibers caused by Rayleigh scattering and multi-phonon processes, the loss limitations in HC-PBGF are primarily from holey interface roughness scattering due to thermally excited surface capillary waves and the anti-crossing between the air guided modes and surface modes [17]. Since holey interface roughness appears to be an intrinsic property in the process of fiber drawing, the loss decrease in HC-PBGF guidance means the field strength decrease of the signal carrying mode at the hole interfaces. One approach is to increase the air core size, which is limited by macro- or micro-bend loss constraints imposed by the undesirable guided modes within the band gaps. As the core size increases, the undesirable guided modes become more plentiful. The modal properties can be altered by proper design of the fiber geometry with a core size given. The most important one is the glass arrangement separating the core and cladding regions. In the process of fabrication, the core surround thickness can be appropriately increased to achieve antiresonance, and the losses dominated by holey interface scattering can be further reduced. Compared with the conventional core surrounds, the antiresonant core surrounds had succeeded in reducing the normalized interface field intensity by a factor 3 and the losses of the fabricated fibers were measured to be as low as 0.0012 dB/m [18]. How-

ever, when the holey interface is smooth and the losses are dominated by mode coupling (it can be achieved by special manufacture technology for the capillary and reasonably controlling the temperature and pressure during the drawing process), fibers with thicker core surrounds show an increased number of mode anti-crossing events due to the larger amount of surface modes generated by truncation of infinite photonic crystal, which will increase the coupling probability between the guided modes and surface modes due to the nearly equivalent propagation constants. These guided modes will leak into the cladding region and gradually attenuate through resonating with the cladding structure including the glass interstitial apexes, the silica structures joining the neighboring apexes, and the air holes. Therefore, it is a better way to decrease the thickness of the core surrounds to reduce the coupling loss. As a matter of fact, the guided modes including the fundamental and higher-order guided modes can constantly happen to couple with the surface modes along the longitudinal direction of HC-PBGF, and the fiber lengths should be appropriately chosen to investigate the propagation characteristics of different guided modes.

4 Conclusion

In summary, the characteristics of band gaps and guided modes of HC-PBGF with interstitial holes at the glass interstitial apexes from near-infrared to visible wavelengths are theoretically and experimentally investigated. The possible degenerate states and loss mechanism of guided modes are elementarily discussed. The further works are primarily concentrated on the detailed analysis of the mode in visible wavelengths and carrying out with the application research of such HC-PBGF on high intensity energy transmission and of special photoelectron apparatus.

Acknowledgements This work is supported by the National High-Technology Research and Development Program of China (2007AA03-Z447) and the Specialized Research Fund for the Doctoral Program of Higher Education (20070013001).

References

1. M. Yan, P. Shum, IEEE Photonics Technol. Lett. **30**, 465 (2005)
2. K.M. Ho, C.T. Chan, C.M. Soukoulis, Phys. Rev. Lett. **65**, 3125 (1990)
3. P. Yeh, A. Yariv, E. Marom, J. Opt. Soc. Am. **68**, 1196 (1978)
4. M. Hentschel, Z. Cheng, F. Krausz, C. Spielmann, Appl. Phys. B **70**, 161 (2000)
5. C. Hauri, W. Kornelis, F. Helbing, A. Heinrich, A. Couairon, A. Mysyrowicz, J. Biegert, U. Keller, Appl. Phys. B **78**, 673 (2004)
6. K.H. Hong, B. Hou, J. Nees, E. Power, G. Mourou, Appl. Phys. B **81**, 447 (2005)
7. R.F. Cregan, B.J. Mangan, J.C. Knight, T.A. Birks, P.St.J. Russell, P.J. Roberts, D.C. Allan, Science **285**, 1537 (1999)
8. G. Bouwmans, F. Luan, J.C. Knight, P.St.J. Russell, L. Farr, B.J. Mangan, H. Sabert, Opt. Express **11**, 1613 (2003)
9. S.O. Konorov, A.M. Zheltikov, P. Zhou, A.P. Tarasevitch, D. von-der Linde, Opt. Lett. **29**, 1521 (2004)
10. F. Couny, F. Benabid, P.J. Roberts, M.T. Burnett, S.A. Maier, Opt. Express **15**, 325 (2007)
11. G. Y Zhou, Z.Y. Hou, L.T. Hou, Appl. Opt. **45**, 1 (2006)
12. M. Miyagi, A. Hongo, Y. Aizawa, S. Kawakami, Appl. Phys. Lett. **43**, 430 (1983)
13. S.P. Guo, A. Sacharia, Opt. Express **11**, 167 (2003)
14. A. Ferrando, E. Silvestre, J.J. Miret, P. Andres, M.V. Andres, Opt. Lett. **24**, 276 (1999)
15. J. Canning, E. Buckley, K. Lyytikainen, T. Ryan, Opt. Commun. **205**, 95 (2003)
16. C.M. Smith, N. Venkataraman, M.T. Gallagher, D. Müller, J.A. West, N.F. Borrelli, D.C. Allan, K.W. Koch, Nature **424**, 65 (2003)
17. R.A. Correa, N.G.R. Broderick, M.N. Petrovich, F. Poletti, D.J. Richardson, Opt. Express **14**, 7974 (2006)
18. P.J. Roberts, D.P. Williams, B.J. Mangan, H. Sabert, F. Couny, W.J. Wadsworth, T.A. Birks, J.C. Knight, P.St.J. Russell, Opt. Express **13**, 8277 (2005)